Available online at www.sciencedirect.com
SCIENCE DIRECT
Journal of Colloid and Interface Science 280 (2004) 409–416
JOURNAL OF Colloid and Interface Science
www.elsevier.com/locate/jcis

Force of a gas bubble on a foreign particle in front of a freezing interface

T. Tao [a], X.F. Peng [a,*], D.J. Lee [b]

[a] *Thermal Engineering Department, Tsinghua University, Beijing 100084, China*
[b] *Department of Chemical Engineering, National Taiwan University, Taipei 10617, Taiwan*

Received 26 March 2004; accepted 3 August 2004

Available online 11 September 2004

Abstract

We monitored the formation and development of a single gas bubble on the surface of a spherical particle of size 1.676 mm under unidirectional freezing and thawing (4.6–5.0 μm/s) and for the first time quantitatively estimated the force exerted on this particle by measuring the deformation of an attached elastic stick. The bubble would nucleate and grow on the particle surface closest to the ice front, while the force curve for a freezing–thawing cycle presented a hysteresis characteristic. This force was much greater than in the case without a bubble, and hence it dominated the engulfment process in the present freezing tests. The bubble force increased with increasing bubble size and was shown to be mainly attributable to the elastic force by the deformed bubble shape. Comments were made on the need to incorporate the role of bubbles in predicting the critical velocity to freeze a suspension with high dissolved gas content.

Keywords: Dissolved gas; Bubble; Freezing; Thawing; Interface; Force

1. Introduction

When an ice front advances in a suspension containing particles, the ice may repel, pierce, break, or entrap the solid particles ahead of it [1–3]. Uhlmann et al. [4] proposed the first systematic analysis on the solid–solidifying front interaction, demonstrating the existence of a critical velocity (V_c) above which all particles would be trapped in the moving front, since a liquid bridge was not maintainable between the particle and the ice front by the surrounding liquid. Other researchers considering particle movement later refined this model [5–7]. The possible effects of process factors such as thermal gradients and surface energy were considered in some recent models [8–14].

In most natural processes and some industrial applications, dissolved gas is present in a vast amount in the suspension. Owing to the very different gas solubilities in the water and ice phases, the dissolved gas tends to be expelled from the solidifying front and be concentrated ahead of the interface. Bubbles were noted to form at the solid–liquid interface in systems with high dissolved gas content [15,16]. The concentration profile of dissolved gas affects the surface-tension gradient around the surfaces of bubbles, hence affecting their entrapment into ice [17,18]. Experimental observation revealed that the gas bubble, once formed, is likely to be trapped as a pore in the solid phase [19–22]. All the work on bubble formation and development at solid–liquid interfaces considered no presence of a foreign particle.

When ice was developed in a suspension with insoluble particles and with high dissolved gas content, bubbles would form not only at the ice–water interface, but also on the particle surface by heterogeneous nucleation. This (these) bubble(s), once formed between the particle and the ice front, would further develop in the concentration boundary layer of the rejected dissolved gas. No works had considered the role of the gas bubbles formed in the particle engulfment process. The measurement of force acting on the particle during freezing and thawing was not reported in the pertinent literature. In this study, we monitored the bubble dynamics on a particle ahead of a freezing front and experimentally estimated the force exerted on the particle by the presence of

* Corresponding author.
E-mail address: djlee@ntu.edu.tw (X.F. Peng).

0021-9797/$ – see front matter
doi:10.1016/j.jcis.2004.08.006

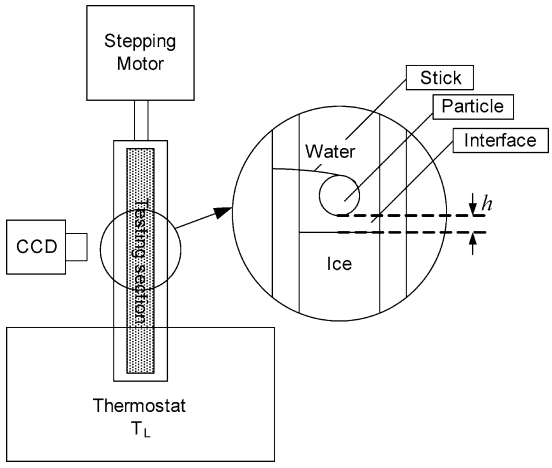

Fig. 1. Schematics of experiment setup.

a vapor bubble. We noted a significant role of the bubble in the particle engulfment process.

2. Experimental

The experimental setup used here resembled the Bridgman freezing tester (Fig. 1), but with a temperature gradient along the vertical direction [23]. The sample was immersed in a freezing pool (HAAKE C35) at −30 °C at a prescribed speed. The test section is a rectangular container made of optical glass of dimensions 25 cm (length) × 11 cm (width) × 5 mm (depth). Ice was allowed to grow upward with a plain interface along the container's length at a prescribed speed ranging from 0.4 to 20 μm/s. In this work the freezing speed (V_i) was fixed at 4.6 μm/s.

A polystyrene sphere of diameter (d_s) 1.676 mm and density (ρ_s) 1043.1 kg/m^3 (measured by an AccuPac 1330 densitometer, Micromeritics, USA) was attached at the tip of an elastic nylon stick (Sundo, Japan) of diameter 148 μm and length 55 mm, which was firmly fixed at the container's side wall and positioned normal to the moving direction of the ice front (along the container's width, Fig. 1). The stick was coated with an impermeable layer to prevent change of properties by moisture swelling. Within the linearly elastic regime the stick deformation is proportional to the applied force; that is, $Y = (1/E)F_s$, where Y (m) is the vertical displacement of the stick tip (with the sphere). The proportionality constant E was estimated before and after the tests as 0.0050 N/m. From the manufacturer's information, the adopted sphere has a thermal conductivity of 0.081 W/(m K) and a heat capacity of 1140 J/(kg K).

A complete test comprised freezing and thawing stages. During the freezing stage, the sphere (with stick) was tracked till it was completely trapped by the ice layer. Following the freezing stage, the direction of container movement reversed to pull the container from the freezing pool. This action induced ice thawing at a prescribed speed. Double-distilled water was the test fluid. During the test a single gas bubble was expected to form via heterogeneous nucleation at the sphere's surface. Hence, for easy observation we needed to expel most dissolved gas in the water to prevent the formation of many bubbles. Before the test the water was degassed by sonicating for 120 min and then boiling for 60 min. Repeated tests revealed that the residual gas thus left could produce at most one gas bubble at the sphere's surface facing an approaching ice front (discussed later).

A digital camera, WAT-505EX (Watec, Japan, 1/3 in., 768 × 576 pixels), equipped with a close-up lens was used to record the stick position. The images, scanned at 768 × 576 pixels per frame, were recorded continuously using the Orine frame grabber (Matrox, USA), sent to a workstation, and analyzed. The vertical displacement of the stick (Y), the ice interface–sphere distance (h), and the bubble size (d_b) were determined with a maximum error of 10 μm.

3. Results and discussion

3.1. Freezing with bubble: observation

Fig. 2 shows a typical freezing and thawing test at a freezing speed of 4.6 μm/s, with black bars as the 1-mm scales. Initially the sphere was far away from the ice front of flat shape (data not shown). As the ice front moved closer to the sphere, owing to the much lower thermal conductivity of the sphere compared with the water (0.611 W/m K), the front became concave downward (Fig. 2a) [24]. A bubble of $d_b = 35$ μm became visible at the position on the sphere closest to the ice front at $h = 135$ μm (Fig. 2b). The bubble had a higher tendency to nucleate at the sphere's surface than at the ice–water interface, as stated in [15]. This bubble kept growing in size while the ice front touched the bubble at $h = d_b = 88$ μm (Fig. 2c). Afterward, the bubble and the sphere were both gradually trapped by the ice front (Fig. 2e), with the bubble growing with time and the sphere pushed upward. At $t > 140$ s (Fig. 2f), the sphere was fixed in space by the ice (Fig. 2h).

In the following thawing stage, it was noticeable that a deformed bubble appeared beneath the bubble in the ice, with a thawed water layer surrounding the bubble (Fig. 2i). The bubble was of a size 3.5 times that of the one just trapped by the ice in Fig. 2d. Therefore, the bubble was able to grow even it was trapped in the ice layer, probably owing to the existence of an unfrozen water layer surrounding the bubble at least over the first several tens of seconds after Fig. 2d. As the ice gradually thawed, the force exerted by the bubble on the sphere could have been so large to make the latter "jump." Afterward, the sphere was pushed downward by the elastic stick with the receding ice front (Figs. 2k–2n). Finally the sphere reached a new equilibrium position at h_f higher than that for Fig. 2a. This difference was attributable to the extra buoyant force from the big bubble that appeared in Fig. 2p. When the attached bubble was removed, the sphere

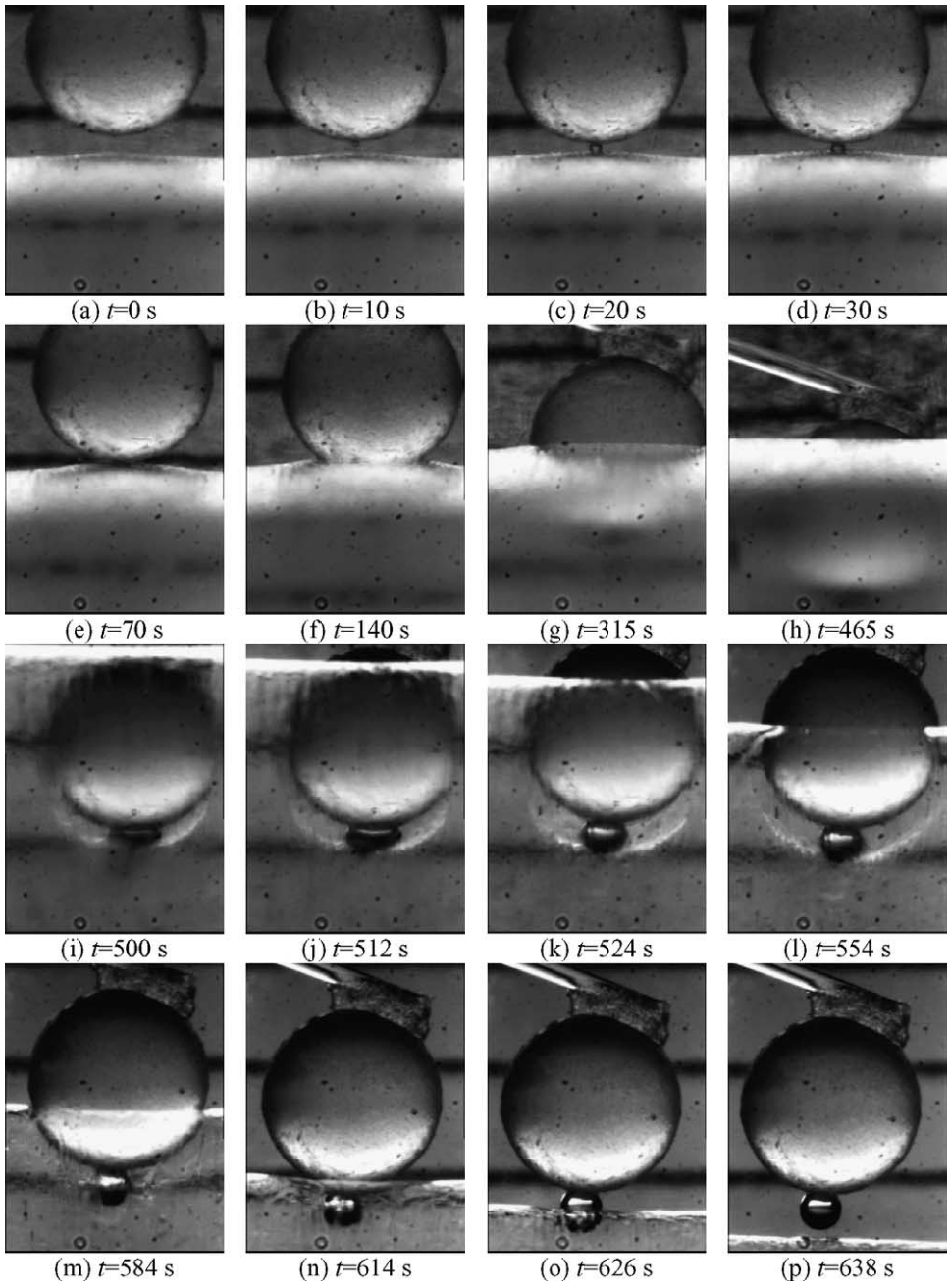

Fig. 2. Typical freezing and thawing test with bubble nucleation. (a)–(h) Freezing stages. (i)–(p) Thawing stages.

was restored to its original position, indicating that the deformation of the stick was within the linear elastic regime and the measurement was reproducible.

Fig. 3 shows a magnified version of the data presented in Fig. 2 on how the bubble was entrapped into the ice. The bubble was nucleated at the sphere's surface closest to the ice front (Fig. 3b), which was attributable to the heterogeneous nucleation of vapor by the rejected dissolved gas from the approaching ice front. The rejected dissolved gas from the ice kept replenishing the formed bubble to increase its size. Finally, the bubble and the ice front met (Fig. 3d). Afterward, the growing ice started to push the bubble, and vice versa. The excess pressure thus produced by the "pressing" action by the bubble would lower the local freezing point of water; hence the ice gradually formed a cavity to entrap the growing bubble (Figs. 3e–3l). This pressure could be of order 10^3–10^4 Pa during freezing. After the sphere was completely trapped and fixed by the ice, the force would not increase further.

3.2. Freezing with bubble: force measurement

The vertical displacement of the stick was estimated using the images recorded in the test, from which the force

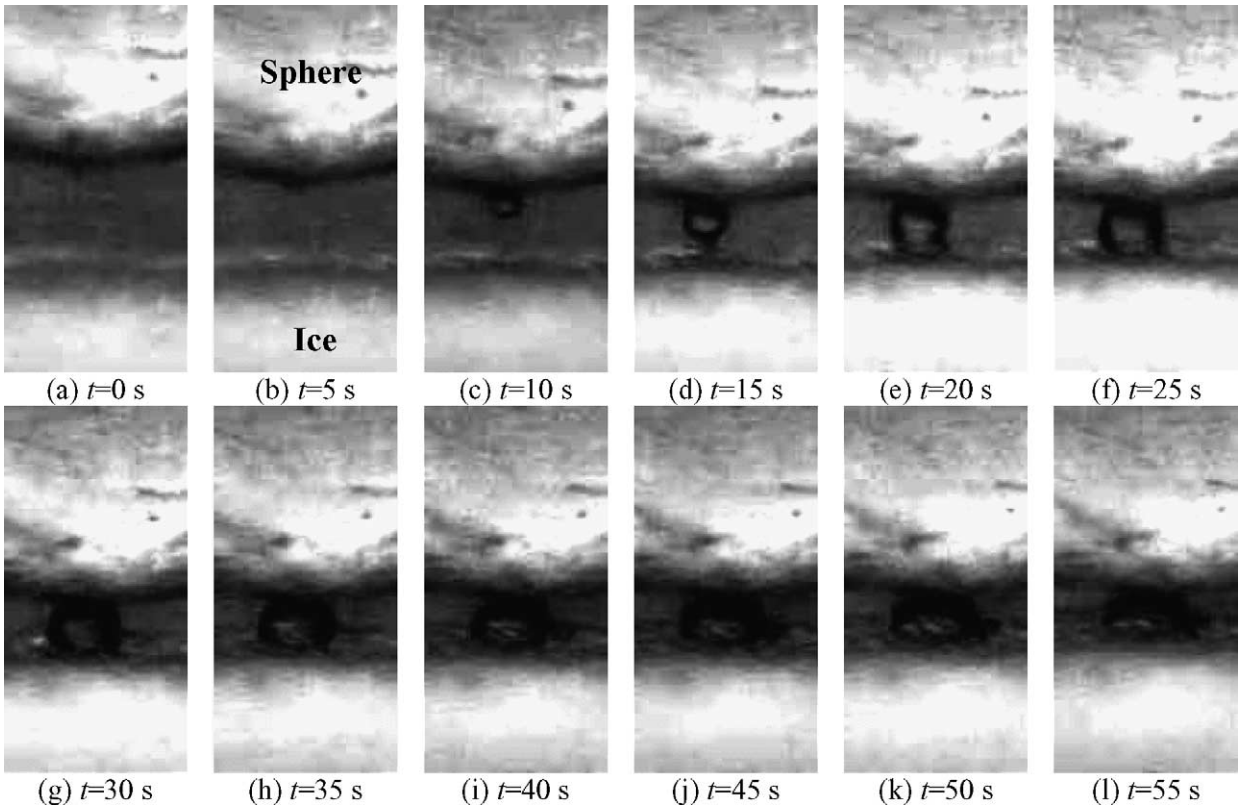

Fig. 3. Bubble growth during freezing process: time interval 5 s, case in Fig. 2.

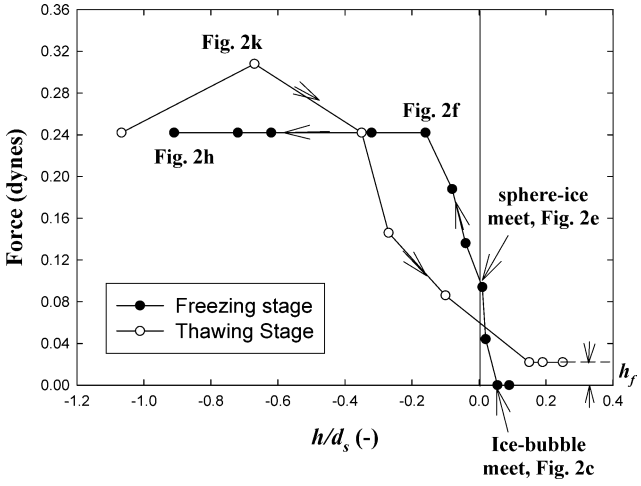

Fig. 4. The force–distance curves for the freeze–thaw cycle. Corresponding to data in Fig. 2.

the stick exerted on the sphere could be calculated based on Hooke's law. Fig. 4 shows the force of the stick on the sphere during the freezing and thawing test in Fig. 2.

When the ice moved toward the sphere, there would be no detectable force from by the stick before the bubble touched the ice (Figs. 2a and 2b). This observation revealed a negligible hydrodynamic drag on the sphere/bubble by the fluid pushed ahead by the ice front. The force became detectable by the stick only if the bubble underneath had touched the ice front (Fig. 2c). This force increased to 9.6×10^{-7} N when the ice met with the sphere (Fig. 2e). Afterward, as the ice continuously trapped the sphere, the force to push up the sphere increased in a nearly linear manner and reached a plateau of 2.42×10^{-6} N till about 16% of the sphere volume was trapped by the ice ($h = -240$ μm).

During the thawing stage, as noted in Fig. 2k, the large bubble formed beneath the sphere would push up the sphere, reaching a force of 3.08×10^{-6} N. Afterward, the receding ice front exerted a lower force on the sphere during its thawing. The action of the big bubble apparently loosened the local ice structure, whose force on the sphere decayed more rapidly than its buildup in the freezing stage. Finally, the buoyant force of the big bubble presented a force on the stick of 2.2×10^{-7} N. This occurrence correlated well with that calculated based on the observed bubble size of 390 μm, around 2.3×10^{-7} N, considering that the attached bubble was not a truncated sphere in shape. Restated, the force–distance curve revealed a hysteresis characteristic. The presence of the nucleated bubble led to distinct freezing and thawing histories.

3.3. Freezing without bubble underneath

Fig. 5 shows a typical freezing and thawing test at the same freezing speed as that in Fig. 2, but with no bubble nucleation on the sphere's surface. In contrast to those noted in Fig. 2, the ice front started to push the sphere only after they met, while the magnitude of vertical displacement was

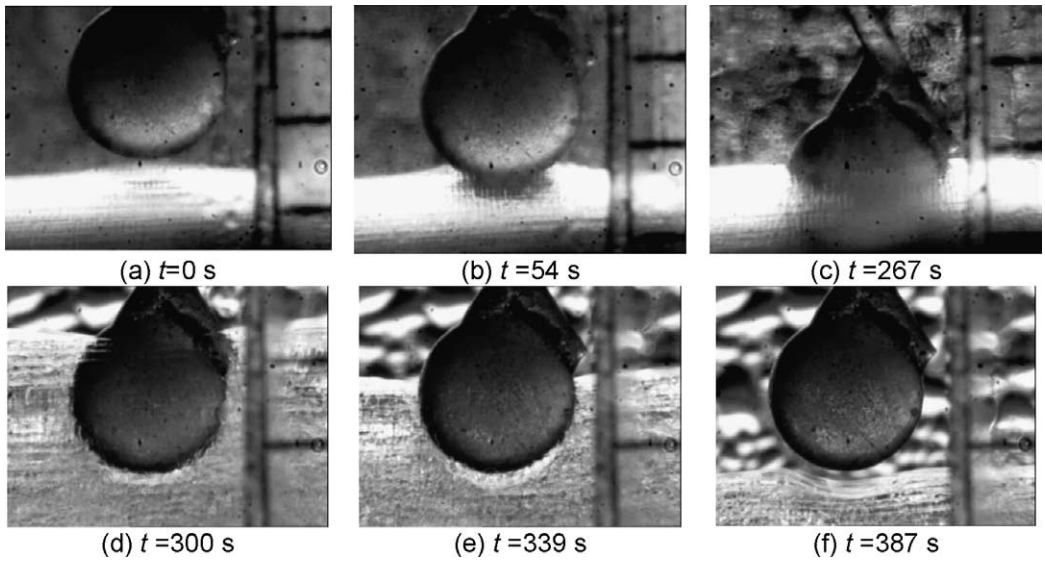

Fig. 5. Typical freezing and thawing test with no bubble nucleation. (a)–(c) Freezing stage. (d)–(f) Thawing stage.

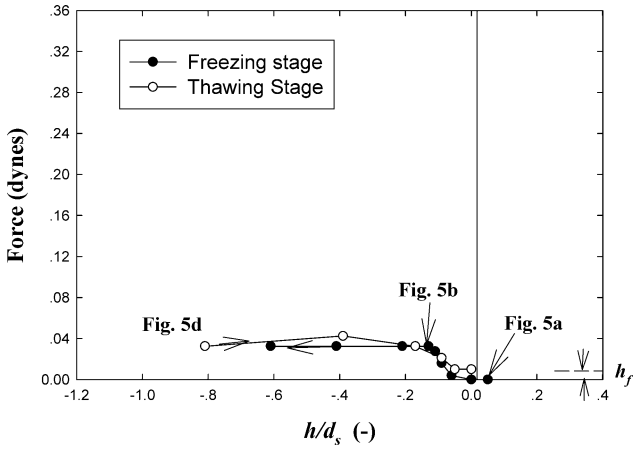

Fig. 6. The force–distance curves for the freeze–thaw cycle, corresponding to data in Fig. 5.

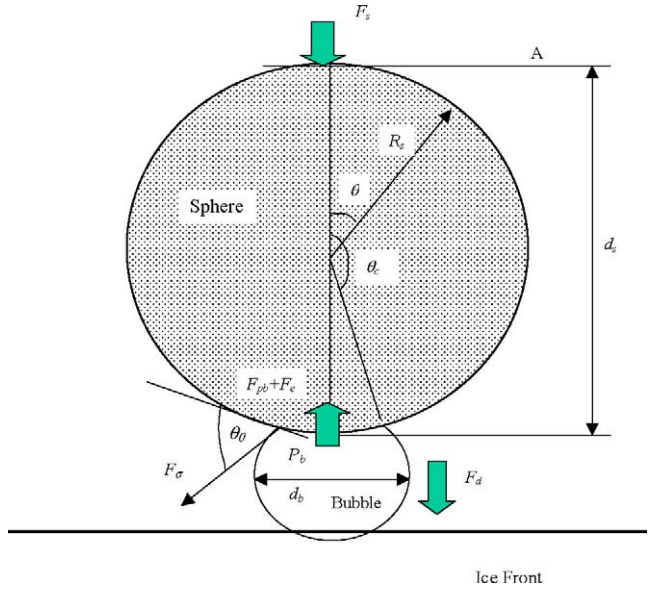

Fig. 7. Schematic of the forces acting on the sphere with bubble underneath.

much milder (Fig. 5c). No large bubble was formed after ice thawing (Figs. 5d–5f).

The force curve in Fig. 6 resembles that in Fig. 2, but with a much lower magnitude. The maximum force over freezing of 3.2×10^{-7} N was only 13% of that depicted in Fig. 2 (2.42×10^{-6} N). Apparently, the force of the bubble on the particle was much higher than the force exerted directly by the ice front without a bubble.

3.4. Force of the bubble

The size of the bubble could not be determined exactly after it was entrapped into ice, owing to the nonspherical, distorted bubble shape and the difficulty of directly observing the bubble through the opaque ice layer. We here take the maximum bubble size observable during freezing as an index for quantitative description of the role of the bubble. (At this stage the sphere had not yet touched the ice front.) Fig. 7 shows the maximum bubble size and the corresponding force data during the freezing stage; for instance, 9.4×10^{-7} N and 155 μm for the case in Fig. 3l. When a big bubble was formed beneath the sphere, the force exerted on the elastic stick was be greater. Moreover, all tests without bubble generation yielded a similar vertical displacement, and then presented a force ranging from 2 to 4×10^{-7} N. This force was what the ice exerted directly on the sphere during freezing without a bubble underneath. The force of the bubble on the particle was much higher than the force exerted directly by the ice front.

Since all tests were conducted at a freezing speed of 4.6 μm/s, an equivalent Reynolds number based on sphere's diameter was less than 0.01. (If the fluid velocity rather than the ice velocity and/or the bubble size rather than the sphere's size were used, the calculated Reynolds number

would be even lower.) Therefore, the inertia effect for the investigated system could be safely ignored and the pseudo-steady-state approximation could be adopted.

The force balance on the sphere (with a bubble sitting beneath) can then be stated as follows (Fig. 7),

$$F_d + F_s + F_\sigma \sin\theta_0 = F_\mu + F_{pb} + F_e, \tag{1}$$

where F_d, F_s, F_σ, F_μ, F_{pb}, and F_e are the disjoining force between the ice front and the sphere due to the nonretarded van der Waals interaction [15], the elastic force by the stick, the surface tension force, the drag force exerted by the fluid pushed ahead by the growing ice front, the net pressure force acting from bubble to the sphere, and the force attributable to the shape deformation of the bubble underneath. The forces F_s, F_μ, and F_d could be estimated as follows.

The force data for $F_s(= EY)$ were measured and demonstrated in Figs. 3 and 5 as examples. The drag force by the fluid (F_μ) and the disjoining force (F_d) by the ice on the sphere could be estimated as follows [4],

$$F_\mu = \pi\mu\left(\frac{V_s}{V_i} - \frac{\rho_l - \rho_i}{\rho_l}\right) V_i \frac{3d_s^2}{2h} \tag{2}$$

and

$$F_d = \frac{A d_s}{12h^2}, \tag{3}$$

where μ is the fluid viscosity, ρ_l and ρ_i are the densities of water and ice, respectively, V_s is the particle moving velocity, and A is the Hamakar constant, ranging from 8×10^{-22} to 6×10^{-21} J for a water–ice system [25]. Moreover, the surface tension force could be evaluated by

$$F_\sigma \sin\theta_0 = 2\pi\left(\frac{d_b \sin\theta_0}{2}\right)\sigma\sin\theta_0 = \pi\sigma d_b \sin^2\theta_0. \tag{4}$$

The net static pressure force from the gas bubble, considering it as a sphere of diameter d_b, could be estimated as follows (F_{pb}),

$$F_{pb} = \int_0^\pi (2\pi R_s \sin\theta)(R_s\,d\theta)\big(-(P - P_A)\cos\theta\big), \tag{5}$$

where $P = P_A + (1-\cos\theta)(R_s\rho_l g)$ over $0 < \theta < \theta_c$, $P = P_b$ at $\theta_c < \theta < \pi$, P_A and P_b are the pressures at the sphere's top and within the bubble, respectively. P_A is taken as a reference pressure and can be removed from the integration. Moreover, the bubble interior pressure can be approximated by $P_b = P_A + (2R_s + R_b)\rho_l g + 2\sigma/R_b$ when R_b is less than R_s. Hence, Eq. (5) becomes

$$F_{pb} = \pi R_s^3 \rho_l g\left\{\frac{2}{3}\big(1-\cos^3\theta_c\big) + \frac{1-\cos2\theta_c}{2}\left[1 + \frac{R_b}{R_s} + 2\frac{(2\sigma/R_b)}{(2R_s\rho_l g)}\right]\right\}. \tag{6}$$

At the limit of no bubble, F_{pb} is equal to the buoyancy force acting on the sphere, a self-evident result. The bubble contributed to the net pressure force since its interior pressure was higher than that of the surrounding liquid by the action of surface tension. In fact, within our experimental range, the last term dominated the static pressure force term, leading to an approximate form of Eq. (6) at $\theta_c \to \pi$ limit as follows:

$$\begin{aligned} F_{pb} &\approx \pi R_s^2\left\{(1-\cos2\theta_c)\frac{\sigma}{R_b}\right\} \\ &\approx \frac{2\pi R_s^2\sigma}{R_b}(\pi-\theta_c)^2 \approx \frac{2\pi R_s^2\sigma}{R_b}\left(\frac{R_b}{R_s}\cos\theta_0\right)^2 \\ &= 2\pi R_b\sigma\cos^2\theta_0. \end{aligned} \tag{7}$$

Taking the case in Fig. 2d as an illustrative example, under this particular condition the elastic force by the stick was 4.6×10^{-7} N. Meanwhile, the corresponding freezing speed was 4.6 μm/s, with $\mu = 1.788\times10^{-3}$ Ns/m^2, $R_s = 8.38\times10^{-4}$ m, $h/2 = R_b = 4.4\times10^{-5}$ m, $\rho_l = 1000$ kg/m^3, $\rho_i = 916$ kg/m^3, $\sigma = 0.076$ N/m, $\theta_0 = 60°$, and $\pi - \theta_c = 3°$ (by experimental observation), giving an estimate of $F_\mu = 1.3\times10^{-10}$ N. $F_\sigma\sin\theta_0 = 1.57\times10^{-5}$ N, $F_{pb} = 5.25\times10^{-6}$ N, and $F_d = 1.8\times10^{-17}$ N. The forces F_μ and F_d were hence much lower than the measured F_s, and Eq. (1) could be simplified for the case with a bubble underneath as follows:

$$\begin{aligned} F_s &\approx F_b = (F_{pb} + F_e - F_\sigma\sin\theta_0) \\ &\approx 2\pi R_b\sigma\big(\cos^2\theta_0 - \sin^2\theta_0\big) + F_e. \end{aligned} \tag{8}$$

Restated, the force measured by the elastic stick roughly estimated the net force exerted by the bubbles underneath on the sphere (F_b). Apparently, if the elastic deformation of the bubble surface could be ignored, $F_s \propto R_b$. Restated, bubble force increases with bubble size.

In the case of no bubble underneath, $F_s = F_\mu - F_d$, which could be estimated as of order 3×10^{-7} N (Fig. 6). Hence, $F_\mu \approx F_d$ and the approximated Eq. (8) was valid as an approximation. The above estimate contains uncertainty since the bubble shape was not perfectly spherical and there existed thermocapillary flow around the bubble (interfacial flow moving toward the ice) that would further modify the bubble shape and the associated pressure field. However, the conclusion that the elastic force measured in the test could properly represent the bubble force remained correct.

Using the measured F_s, R_b, and θ_0 data, the contribution of F_e could be estimated using Eq. (8). Taking Fig. 2e as an example, where $F_s = 1.39\times10^{-6}$ N and $R_b = 88$ μm, $F_e = 2.24\times10^{-5}$ N, being one order of magnitude higher than F_s. The competition between F_σ, F_{pb}, and F_e yielded the net bubble force, F_b. Regardless of the origin of F_b, it presented the controlling factor determining the force field on the sphere.

3.5. Particle entrapment

In most natural processes and in some industrial applications the dissolved gas content in water is high. During freezing, the dissolved gas would be expelled and be concentrated

ahead of the ice front owing to the great difference in its solubilities in the water and ice phases. When a foreign particle existed in front of a freezing front, heterogeneous nucleation would easily occur at the solid surface closest to the freezing front, where the gas supersaturation was the highest. Once the bubble was heterogeneously nucleated on the sphere bottom, as demonstrated in the preceding sections, its development controlled the force field on the sphere. This maximum force of the ice front has practical significance: if the sphere could not resist this force (for instance, by the stick applied in this test), it would be pushed away by an acceleration determined by the particle mass and the fluid viscosity. In such a case, whether or not the particle would be entrapped by the growing ice front would depend on how fast it ran away and how fast the ice front caught up. A competition occurred between the ice front and the escaping sphere for entrapment. In the particular case studied in the present work, the acceleration of the particle to move upward with the biggest bubble detected in Fig. 2 would be an order of magnitude larger than that without a bubble.

The heterogeneous nucleation of gas depends on local gas supersaturation and the surface characteristics of the particle, which are of a stochastic nature and discourage the search for a definite critical velocity for a natural suspension. Hung et al. [26] demonstrated that the solid rejection ratio for an activated sludge system increases continuously with decreasing freezing speed. This occurrence may also be attributable to the formation of gas bubbles on the sludge flocs under freezing.

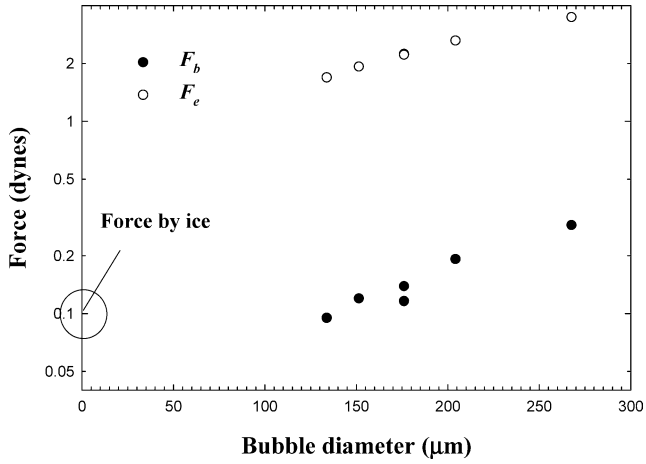

Fig. 8. Forces versus bubble size at the moment ice touched the sphere.

4. Conclusions

Bubbles would be formed on the particle surface when the particle was placed in front of a solidifying ice front with high dissolved gas content. We monitored the formation and development of a single gas bubble on the surface of a spherical particle of size 1.676 mm under unidirectional freezing and thawing (4.6 μm/s) and quantitatively estimated the force exerted on the particle by measuring the deformation of an elastic stick attached on it. Experimental results revealed that the formed bubble started to push the particle apart when it touched the ice front. The force exerted on the particle was built up in strength until the ice layer had trapped about 1/6 of the sphere's volume. For the first time, this "bubble force" was estimated as 2.42×10^{-6} N (max.) in a typical freezing test, which was much higher than the force exerted directly by ice in a test without a bubble ($2–4 \times 10^{-7}$ N). The force of the bubble increased with increasing bubble size (see Fig. 8).

The force of the bubble dominated the particle engulfment in freezing. During thawing, the force curve followed a distinct path from that in the freezing test, with its value increased suddenly to 3.08×10^{-6} N owing to the formation of a big gas bubble underneath the sphere. The present study revealed that neither the drag force exerted by the fluid pushed ahead by the growing ice front nor the van der Waals disjoining force was significant to the investigated process. The origin of the bubble force was mainly attributable to the surface tension force, the static pressure force, and the elastic force from bubble shape deformation.

Since in most natural processes and in some industrial applications the dissolved gas content in suspension is high, bubble formation is inevitable when these suspensions are subjected to freezing. The force exerted by the bubble on the foreign particle has to be taken into account when searching for the critical velocity to freeze these suspensions.

Acknowledgments

This research is currently supported by the National Natural Science Foundation of China (Contract 50136020). T. Tao is grateful to National Taiwan University for inviting him as an exchange student during November 2003–March 2004.

Appendix A. Nomenclature

A	Hamakar constant (J)
d_b	diameter of bubble (m)
d_s	diameter of sphere (m)
E	proportionality constant (N/m)
F_b	force from bubble (N)
F_d	disjoining force (N)
F_e	elastic force from bubble (N)
F_pb	net static pressure force (N)
F_s	force from stick (N)
F_σ	surface tension force (N)
F_μ	drag force (N)
g	gravitational acceleration (m/s^2)
h	distance between sphere and ice front (m)
h_f	final equilibrium height (m)

P	pressure (Pa)
P_A	pressure at sphere's top (Pa)
P_b	interior pressure of bubble (Pa)
R_b	radius of bubble (m)
R_s	radius of sphere (m)
t	time (s)
V_c	critical velocity (m/s)
V_i	velocity of ice front (m/s)
V_s	velocity of sphere (m/s)
Y	vertical displacement of stick (m)
θ	angular coordinate (–)
θ_c	angular angle of contact area (–)
θ_0	contact angle (–)
μ_l	liquid viscosity (Pa s)
ρ_i	density of ice (kg/m^3)
ρ_l	density of water (kg/m^3)
ρ_s	density of sphere (kg/m^3)
σ	surface tension (N/m)

References

[1] H. Ishiguro, B. Rubinsky, Cryobiology 31 (1994) 483.
[2] G. Gay, M.A. Azouni, Cryst. Growth Design. 2 (2002) 135.
[3] L. Hadji, Eur. Phys. J. B 37 (2004) 85.
[4] D.R. Uhlmann, B. Chamlers, K.A. Jackson, J. Appl. Phys. 35 (1964) 2986.
[5] G.W. Delamore, R.W. Smith, A.F.S. Trans. 79 (1971) 560.
[6] R.W. Smith, G.W. Delamore, W.B.F. Mackay, A.F.S. Trans. 80 (1972) 299.
[7] Q. Han, J.D. Hunt, J. Cryst. Growth 152 (1995) 221.
[8] P. Hoekstra, R.D. Miller, J. Colloid Interface Sci. 25 (1967) 166.
[9] G.F. Bolling, J. Cisse, J. Cryst. Growth 10 (1971) 67.
[10] J.K. Kim, P.K. Rohatgi, Metall. Mater. Trans. A 29 (1991) 351.
[11] D.M. Stefanescu, B.K. Dhindaw, S.A. Kacar, A. Moitra, Metall. Trans. A 19 (1990) 2847.
[12] D. Shangguan, S. Ahuja, D.M. Stefanescu, Metall. Trans. A 23 (1992) 669.
[13] J. Potschke, V. Rogge, J. Cryst. Growth 152 (1995) 221.
[14] J.W. Garvin, H.S. Udaykumar, J. Cryst. Growth 252 (2003) 467.
[15] P.S. Wei, C.C. Huang, K.W. Lee, Metall. Mater. Trans. B 34 (2003) 321.
[16] G. Lipp, C. Korber, S. Englich, U. Hartmann, G. Rau, Cryobiology 24 (1987) 489.
[17] Z. Wang, K. Mukai, I.J. Lee, ISIJ Int. 39 (1999) 553.
[18] M.A. Rogerson, S.S.S. Cardoso, J. Fluid Mech. 419 (2000) 263.
[19] P.S. Wei, C.Y. Ho, Metall. Mater. Trans. B 33 (2002) 91.
[20] P.S. Wei, Y.K. Kuo, S.H. Chiu, C.Y. Ho, Int. J. Heat Mass Transfer 43 (2000) 263.
[21] K. Murakami, Y. Nakai, H. Nakajima, Int. J. Cast Met. Res. 15 (2002) 459.
[22] K. Murakami, H. Nakajima, Mater. Trans. 43 (2002) 2582.
[23] B. Rubinsky, M.A. Ikeda, in: C.-L. Tien, A. Majumdar, F.M. Gerner (Eds.), Microscale Energy Transport, Taylor & Francis, Washington, DC, 1998.
[24] P. Cases, M.A. Azouni, J. Cryst. Growth 130 (1993) 13.
[25] J.N. Israelachvili, Intermolecular and Surface Forces, second ed., Academic Press, San Diego, 1991.
[26] W.T. Hung, I.L. Chang, W.W. Lin, D.J. Lee, Environ. Sci. Technol. 30 (1996) 2391.